ACS APPLIED MATERIALS & INTERFACES

Research Article

www.acsami.org

Flexible Three-Dimensional SnO_2 Nanowire Arrays: Atomic Layer Deposition-Assisted Synthesis, Excellent Photodetectors, and Field Emitters

Kaimo Deng,* Hao Lu, Zhiwei Shi, Qiong Liu, and Liang Li*

Department of Physics, Jiangsu Key Laboratory of Thin Films, Soochow University, Suzhou 215006, P. R. China

ABSTRACT: Flexible three-dimensional SnO_2 nanowire arrays were synthesized on a carbon cloth template in combination with atomic layer deposition and vapor transport. The as-grown nanostructures were assembled by high density quasi-aligned nanowires with a large aspect ratio. Nanoscale photodetectors based on the flexible nanostructure demonstrate excellent ultraviolet light selectivity, a high speed response time less than 0.3 s, and dark current as low as 2.3 pA. Besides, field emission measurements of the hierarchical structure show a rather low turn-on field (3.3 Vμm^{-1}) and threshold field (4.5 Vμm^{-1}), as well as an excellent field enhancment factor (2375) with a long-term stability up to 20 h. These results indicate that the flexible three-dimensional SnO_2 nanowire arrays can be used as functional building blocks for efficient photodetectors and field emitters.

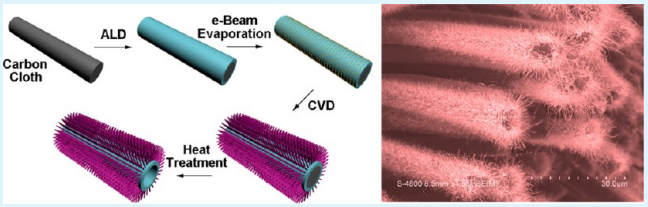

KEYWORDS: *flexible, SnO_2, nanowire arrays, photodetectors, field emitters*

INTRODUCTION

The development of growth techniques for semiconductor nanowires provides possibilities in designing nanostructures with desired composition, heterojunctions, and architectures.[1,2] Benefiting from this, semiconductor nanowires have been widely investigated as building blocks for optoelectronic devices, including photodetectors,[3−5] field emitters,[6−8] gas sensors,[9,10] microcavity lasers,[11] and solar cells.[12−14] The unique optoelectronic and geometry properties of nanowires allow them to serve a dual function as active elements and interconnections, thus leading to well integrated devices and shrinking of devices to a small length scale. In the context of future development toward thinner, lighter, and cheaper solutions, flexible optoelectronic devices have recently attracted extensive attention since they hold great promise in applications of wearable solar cells, energy storage, and stretchable liquid crystal display.[15−19] Semiconductor materials are typically deposited on flexible substrates such as metal mesh, carbon cloth, and polyethylene terephthalate to achieve the required performance. To date, there has been much effort devoted to the synthesis of flexible nanostructures for energy harvesting and storage based on carbon cloth, due to the distinctive properties, such as high strength, conductivity, and stability, over other counterparts.[15−17] Especially, the carbon cloth is also favored for the fact that it can be readily removed by heat treatment in air. An alternative method to develop flexible electronics is utilizing flexible semiconductor materials instead where a supporting substrate is not necessary.

Of all the metal oxide semiconductors investigated as fundamental elements for optoelectronic devices, tin dioxide (SnO_2), an *n*-type semiconductor, is considered to be one of the most advantageous candidates.[20,21] The optical and electronic properties of this material are unique in two respects. On the one hand, SnO_2 exhibits a direct bandgap (3.6 eV) and is transparent to visible light, which makes it an ideal material for visible-blind photodetectors. It is also demonstrated that nanostructured devices have advantages of faster response time and compactness compared with bulky technologies. Although various SnO_2 nanostructures such as nanowires, nanowire arrays,[22−25] nanobelts,[26] and nanonets[27] have been fabricated and tested for photodetectors, the dark current and response time of these SnO_2 nanostructure based devices are still unsatisfactory. Thus, it still remains to be a grand challenge to optimize the structural design that may greatly improve the response time and the photocurrent while decreasing the dark current. On the other hand, SnO_2 can also find its application in field emission since it has a relatively low work function (4.7 eV) in contrast with carbon nanotube (5 eV) and ZnO (5.3 eV). To date, there are, however, limited reports of field emission properties of SnO_2 nanostructures.[28−33] Meanwhile, these devices suffer from a fair field enhancement factor as well as high threshold and turn-on fields. As the most important figures of merit for the device, they are far below expectation and need further improvement for applications.

In this paper, we reported, for the first time, successful synthesis of flexible three-dimensional (3D) SnO_2 nanowire arrays on a carbon cloth template and demonstrated such a hierarchical nanostructure can greatly enhance the performance of photodetector and field emitter. The novel 3D nanostructures were synthesized by combined processes of atomic layer

Received: May 10, 2013
Accepted: July 23, 2013
Published: July 23, 2013

   dx.doi.org/10.1021/am401762y | ACS Appl. Mater. Interfaces 2013, 5, 7845−7851

deposition (ALD) and vapor transport. Figure 1 schematically illustrates the synthesis process, involving a thin SnO_2 layer

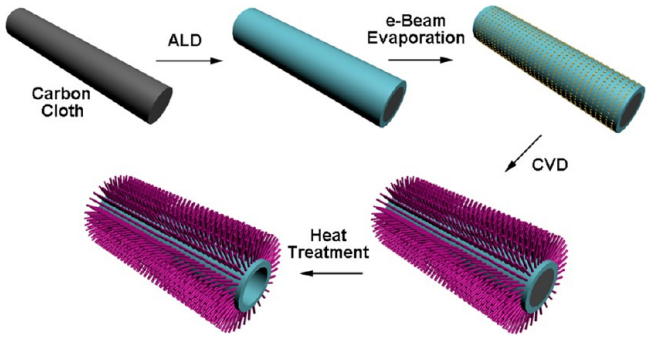

Figure 1. Schematic showing the fabrication process of the 3D SnO_2 nanostructure on a carbon cloth template. A thin SnO_2 layer is first deposited on carbon fiber with ALD. Then, Au nanoparticle film catalyst is formed by electron beam evaporation followed by the vapor transport deposition of SnO_2 nanowire arrays. Finally, the carbon cloth is removed by postheat treatment.

deposition on carbon cloth by ALD followed by introducing an Au thin film as the catalyst through electron beam evaporation, the vapor transport deposition of SnO_2 nanowire arrays, and the postheat treatment to form the flexible nanostructure. The photodetector based on as-grown 3D SnO_2 nanostructure exhibited excellent light selectivity and response time lower than 0.3 s. More intriguingly, the dark current by applying a voltage of 1.0 V was only 2.3 pA, several orders of magnitude lower than that of previously reported SnO_2 nanostructured devices. Field emission measurements showed a rather low turn-on field (3.3 Vμm^{-1}) and threshold field (4.5 Vμm^{-1}), as well as an excellent field enhancement factor (2375) with a long-term stability up to 20 h, which surpass the performance of existing SnO_2 field emitters. These parameters undoubtedly reveal the advantage of the 3D SnO_2 nanowire arrays as functional building blocks.

EXPERIMENTAL SECTION

Material Preparation and Characterization. A piece of carbon cloth was cleaned by sonication with acetone, ethanol, and deionized water in sequence, and each session lasted 30 min. Prior to the nanowire growth by vapor transport in a tube furnace, a SnO_2 thin layer was deposited on the carbon cloth by atomic layer deposition followed by a Au thin layer deposition through electron beam evaporation as a catalyst for the growth of aligned SnO_2 nanowire arrays. A small quartz tube with one end open was loaded with pure SnO_2 powder and placed at the center of the furnace, and the substrate was located near SnO_2 powder at the downstream of the Ar gas flow (350 standard cubic center meter). The furnace temperature was increased to 760 °C at a heating rate of 20 °C min^{-1} and kept constant for 1.5 h. After cooling down to room temperature in the flowing carrier gas, the sample received heat treatment at 800 °C in air for 1 h to get the final products. The as-prepared samples were characterized by X-ray diffraction (XRD, Ultima IV/PSK), scanning electron microscopy (SEM, Hitachi S-4800), and transmission electron microscopy (TEM, JEM-3000F).

Device Fabrication and Measurement. 3D SnO_2 nanostrucutured photodetector was assembled by using Au microwire as a mask: (1) 3D SnO_2 nanowire array was transferred onto a SiO_2/Si substrate. (2) Next, an Au microwire with a diameter of 30 μm was

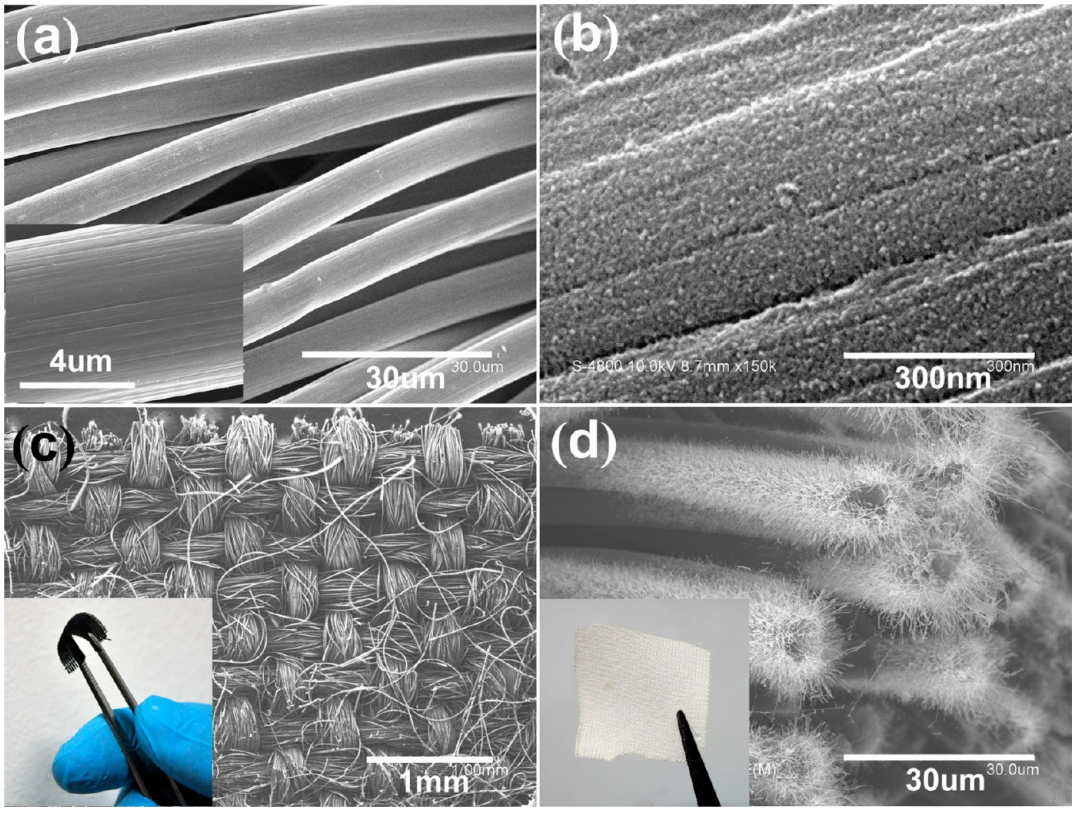

Figure 2. (a and b) SEM images of carbon fiber before and after a SnO_2 thin layer decoration by ALD. (c) Top view SEM image of carbon cloth that underwent vapor transport treatment. Inset: Optical image of the carbon cloth with SnO_2 nanostructures. (d) Cross-sectional SEM image of as-synthesized 3D SnO_2 nanowire arrays with postheat treatment. Inset: Optical image of the SnO_2 hierarchical structure after heat treatment.

used to shade a part of 3D SnO_2 nanostructure. (3) Then, a Ti/Au (50 nm/200 nm) film was formed by electron-beam deposition to cover the entire surface of the substrate. (4) The last step was to remove the Au microwire. An Advantest picoammeter (R8340A) and a dc voltage source (R6144) were employed to record the current−voltage (I−V) curves of the photodetector by a two-probe method. The response of the photodetector under light illumination of different wavelengths was measured by a 500 W Ushio xenon lamp equipped with an Acton Research monochromator. Light intensity was calibrated by a UV-enhanced Si photodiode, and tunable light intensities were available by modulating the size of the aperture. The intensity of 350 nm UV light was 1.44 mW cm^{-2}, and the distance from the photodetector to UV lamp was 2.0 cm. Before measurements, we did not perform any activation process. Once the surface of nanowires was illuminated by the vertically incident light, the photocurrent was recorded automatically by a computer.

The 3D SnO_2 nanostrucutures were directly affixed onto a Cu cathode and a Cu prober with a cross-section of 1 mm^2 served as the anode. The applied dc voltage to the samples was scanned from 100 to 1100 V, and the resulting current was detected simultaneously. All the field emission measurements were carried out in a vacuum chamber under a low pressure of 5×10^{-6} Pa. Dividing the recorded current by the effective emission area yielded the current density (J), while the macroscopic electric field (E) was defined as the ratio between the applied voltage and the distance of anode and cathode (V/d).

RESULTS AND DISCUSSION

The morphology image characterized by scanning electron microscopy (SEM) in Figure 2a shows that the carbon fiber is about 10 μm in diameter and has a smooth surface. It is noted that ALD resulted in a uniform SnO_2 nanoparticle film on the surface of carbon fiber, as manifested by Figure 2b. Particularly, the introduction of a thin SnO_2 layer before the growth of nanowire arrays is to maintain the structural stability in case of the removal of the carbon cloth template. As expected, the carbon cloth that has undergone the vapor transport process preserves the flexibility and large-scale structure as shown in Figure 2c. After postheat treatment, it can be seen from a cross-sectional view in Figure 2d that a hollow hierarchical structure is obtained. Narrow diameter distributed and high-density nanowire arrays align vertically on the surface of the thin SnO_2 layer. The length of the nanowires is found to be about 5 μm. In the absence of the carbon cloth template, the hierarchical structure still remains intact without destroying its original morphology and we can even pick it up with great care (inset of Figure 2d). According to the vapor−liquid−solid growth mechanism, unidirectional SnO_2 nanowire growth is promoted by the presence of metallic catalysts, where Au forms its liquid alloy combined with vaporized growth sources. Similar results were also obtained in previous literature.[34−36] The XRD patterns of the nanostructure are depicted in Figure 3. All the diffraction peaks can be well indexed to the tetragonal rutile phase of tin oxide (JCPDS 77-0477). The relative intensity, however, deviates from that of the standard data as a result of a different oriented growth direction.[37] A weak and broad peak in the small angle region arises from the glass sample holder used in XRD measurement.

The microstructure of the SnO_2 nanowire was further checked by transmission electron microscopy (TEM). Figure 4a,b presents the TEM image of a single nanowire and its high-resolution image along with the selected area electron diffraction (SAED) pattern taken at a random position, respectively. The nanowire has a diameter of around 60 nm. The spacing of the lattice fringes measured from Figure 4b is about 0.26 nm, which corresponds to the (101) plane of rutile

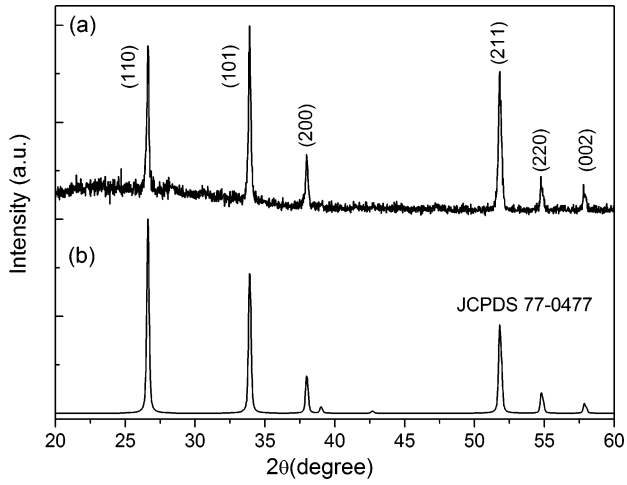

Figure 3. XRD patterns of (a) the 3D SnO_2 nanostructure with postheat treatment and (b) standard data from JCPDS 77-0477.

SnO_2 and is consistent with the SAED pattern (Figure 4b, inset). Both the clear lattice fringe and the sharp contrast of the electron diffraction pattern indicate the good crystallization of the nanowire. A close study of the high-resolution TEM image suggests that the nanowire grows along the $[11\bar{2}]$ crystal direction. In addition, a detailed chemical analysis was conducted by elemental mapping as shown in Figure 4c,d. It is apparent that the nanowire has a homogeneous distribution of compositional elements (Sn and O), further confirming the uniform microstructure.

Figure 5a shows the spectral response of the photodetector at 1 V bias under constant light intensity. The as-fabricated device has a pronounced photocurrent in the UV region with a cutoff wavelength of ~350 nm, whose energy is close to the bandgap of SnO_2, suggesting the bandgap excitation is responsible for the photoresponse process. As the wavelength decreases, the responsivity, typically defined as the ratio between the photocurrent and the incident light power, increases gradually and the maximal value is obtained at ~250 nm. An interpretation about the photoresponsivity of the detector can be made in terms of the logarithmic scale graph in Figure 5b. We notice that the as fabricated photodetector offers a higher selectivity toward UV illumination, since the responsivity around 250 nm is about 3 and 4−5, respectively, orders of magnitude larger than the value in the cutoff wavelength and the visible region. However, a clear drop in responsivity is observed at shorter wavelengths, which are ascribed to two possible factors. First of all, the spectral response experiment is conducted under constant light intensity, and there will be a smaller number of photons available at shorter wavelengths to excite electron−hole pairs. Second, because high-energy light has a large absorption coefficient, it is strongly absorbed in a short distance below the surface. The photoexcited electron−hole pairs in the surface region have a shorter lifetime than that in the buck and thus play a minor role in photoconductivity.[38]

Figure 5c represents the current−voltage (I−V) curve of the photodetector under light illumination of different wavelengths or dark condition. The dark current of the device is only 2.3 pA (1.0 V), a value much lower than those in the previously reported literature (see Table 1). The photoexcited current is much higher than the dark current, and the photocurrent can reach to 0.5 nA under 350 nm light illumination by applying a low voltage of 1.0 V. A larger photocurrent can be detected at a

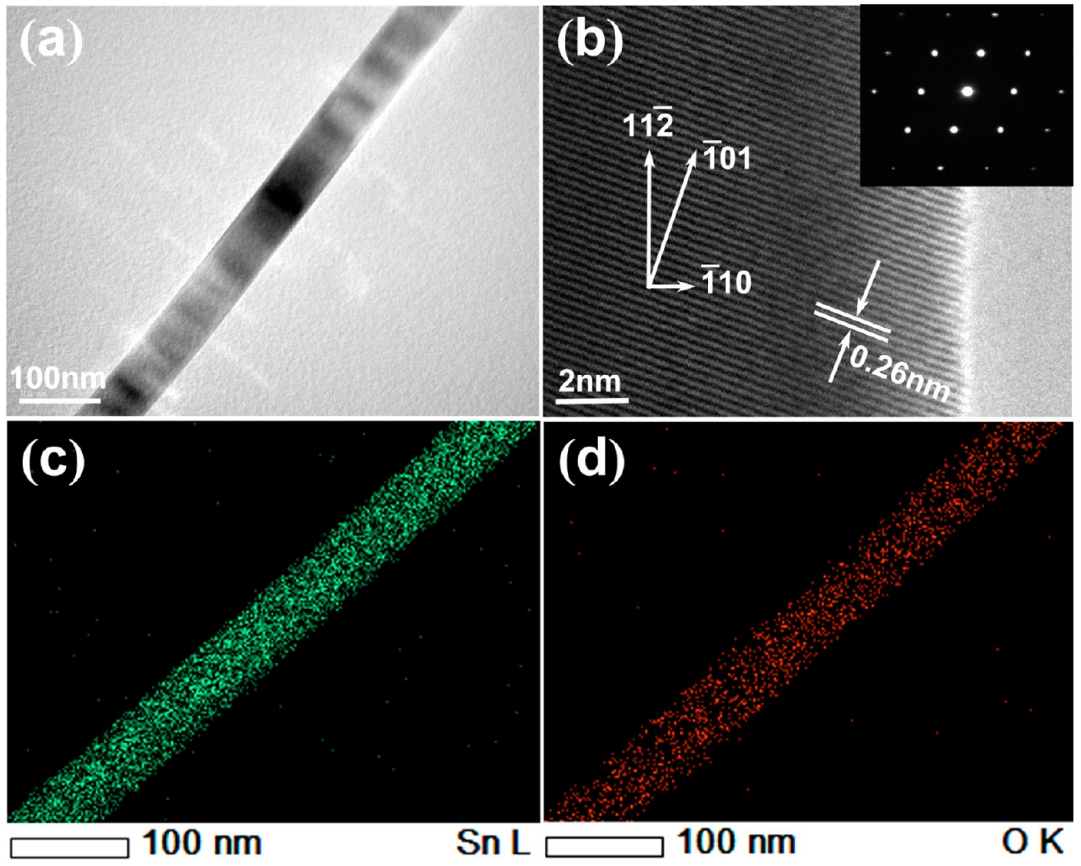

Figure 4. (a) Representative TEM image of an individual SnO_2 nanowire. (b) Corresponding high-resolution TEM image, showing the single crystalline structure. Inset shows a SAED pattern. (c and d) Element maps for Sn and O, respectively.

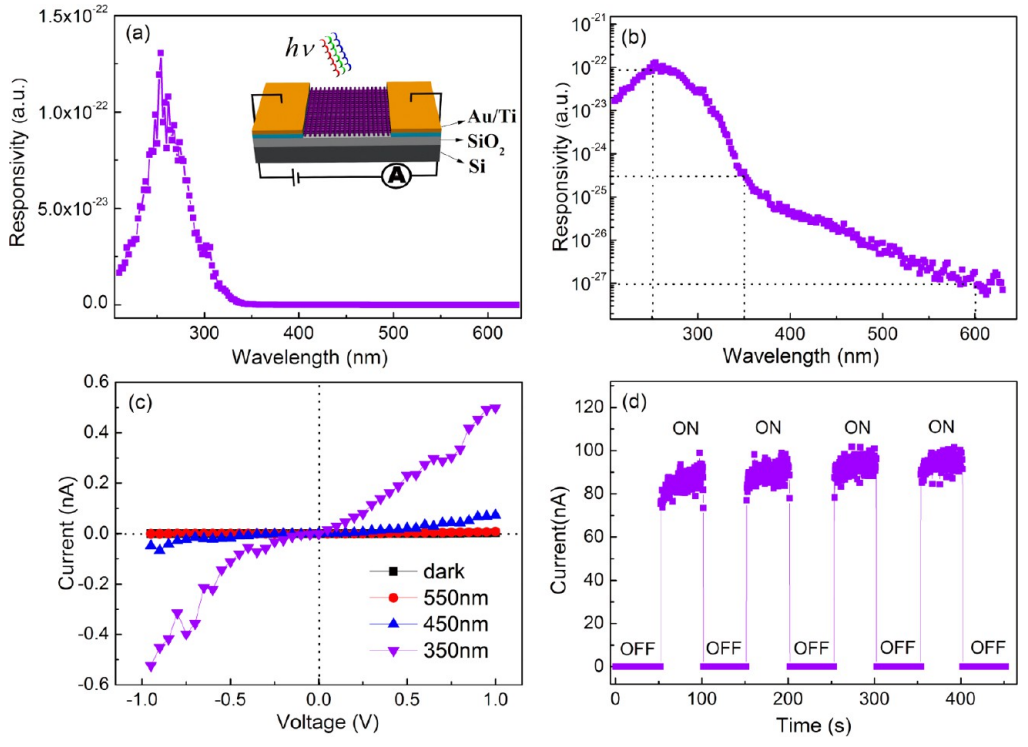

Figure 5. (a) Spectral response of 3D SnO_2 nanostructured photodetector, demonstrating a cutoff wavelength around 350 nm. Inset shows a schematic diagram of the device. (b) Logarithmic plot of spectral response. (c) *I*–*V* curves under light illumination of different wavelengths or dark condition. (d) Time response of the photodetector.

Table 1. Comparison of the Key Parameters of SnO_2 Nanostrucuture Based Photodetectors between This Work and Previous Studies

SnO_2 nanostrucuture	dark current	response time	reference
nanowire	40 nA (0.1 V)	several seconds	22
nanowire	19.4 nA (1 V)	several seconds	23
Sb-doped nanowire	2pA (1 V)	1 s	24
nanowire array	77 μA (12 V)	several seconds	25
nanobelts	0.4 nA (−5 V)	1 s	26
nanonet	66 μA (1 V)	several seconds	27
3D nanowire arrays	2.3 ± 0.3 pA (1 V)	<0.3 s	present work

higher bias. It is widely accepted that oxygen chemisorptions play a vital role in regulating the UV sensitivity. In dark condition, oxygen molecules adsorb on the surface and capture free electrons from SnO_2, therefore forming a low conductive depletion layer in the surface region. Under UV light exposure, photoexcited holes migrate to the surface and discharge the adsorbed oxygen ions (negatively charged) through electron−hole recombination,[39] leading to the enhanced conductivity.

To explore its potential for optoelectronic switches, we have plotted the response of the photodetector versus time in Figure 5d by periodically turning on and off the UV source (350 nm) at a bias of 10 V. The current intensifies rapidly under illumination to a constant value (about 90 nA) and then drops abruptly to its original state when turning off the light, with on/off ratio up to 10^5. Both the response time and decay time are extremely short, and they are below the detection limit (0.3 s) of the ampermeter used in our experiments. Such a fast response is superior to the performance of those devices in earlier reports.[22−27] The improved photoresponse is probably due to a considerable amount of nanowire/nanowire junctions formed between neighboring nanowires in the nanostructure, where they act as Schottky-like junctions and electrical conducting paths for electrons.[40] All the above results indicate that the present photodetector features low dark current, high speed response, and good sensitivity in the UV region and can serve as highly sensitive UV light detectors.

Field emission properties of the as-synthesized 3D SnO_2 nanowire arrays were also investigated. A schematic diagram of the as-fabricated field emitter based on the SnO_2 hierarchical structure is shown in Figure 6a, where the inset presents the optical image of flexible functional building block by affixing the SnO_2 hierarchical structure on a conductive tape. Figure 6b depicts the field emission current density J as a function of the applied field E with two electrodes separated by 200 μm. The electron emission turn-on and threshold field, typically defined as the macroscopic electric field necessary to obtain a current density of 10 and 1 mAcm^{-2}, respectively, are about 3.3 and 4.5 Vμm^{-1}. With increased applied field, the electron emission current increases exponentially. In order to better understand the emission properties, the J−E data were fitted by Fowler-Nordheim (FN) theory[41−43] described by

$$J = (A\beta^2E^2/\Phi)\exp(-B\Phi^{3/2}/\beta E) \quad (1)$$

where Φ and β represent the work function and the field-enhancement factor, respectively. A (1.54×10^{-6} AeVV^{-2}) and B (6.83×10^3 eV$^{-3/2}$Vμm^{-1}) are constant values. The local electric field (E_{loc}) and the macroscopic electric field E accord with a linear relation: $E_{loc} = \beta E$. By plotting $\ln(J/E^2)$ as a function of $1/E$, we can obtain a FN relation (Figure 6b, inset).

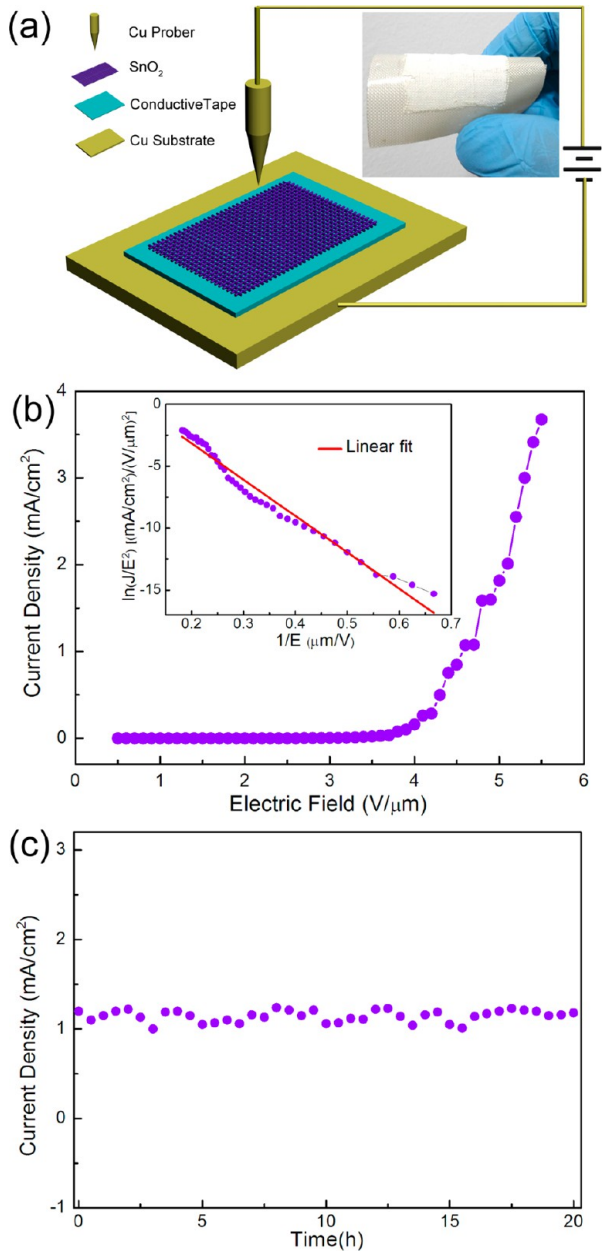

Figure 6. (a) Schematic diagram of the field emitter based on the SnO_2 hierarchical structure. Inset: Optical image of the flexible functional building block by affixing the SnO_2 hierarchical structure on a conductive tape. (b) The field-emission current density J as a function of the applied field E with two electrodes separated by 200 μm. The inset is a $\ln(J/E^2) - 1/E$ plot from the Fowler-Nordheim equation. (c) Stable field emission current recorded over 20 h.

The conventional field emission mechanism is manifested by the linearity of the fitted curve. The β value calculated from the slope of the fitted curve is as high as 2375. We attributed such an excellent field emission performance to the extremely high-density, quasi-aligned arrangement and a large aspect-ratio of SnO_2 nanowires. The stability of the SnO_2 nanostructure is also remarkable. During 20 h of continuous operation at 1 mAcm^{-2}, no large current degradation and obvious fluctuation can be found. The long-term field emission stability enables the present 3D SnO_2 nanostructure to be a promising candidate for flat panel display. As far as we know, present field emitters have

Table 2. Comparison of the Field Emission Parameters between This Work and Previous Studies of SnO_2 Nanostrucutures[a]

SnO_2 nanostrucuture	turn-on field (V/μm)	threshold field (V/μm)	enhancement factor	reference
quasi-aligned nanowires	3.5	4.63	1225	28
nanowire	2.3 at 0.1 μAcm^{-2}	6.5	2772	29
nanobelt	1.9 at 0.1 μAcm^{-2}	5.1	3178	29
nanobelt arrays	4.5 at 1 μAcm^{-2}		950	30
nanorod	6.4		493.6	31
nanograss	5.61 at 1.44 μAcm^{-2}		1477	32
3D nanowire arrays	3.3 ± 0.2	4.5 ± 0.1	2375 ± 3	present work

[a]The electron emission turn-on and threshold field are typically defined as the macroscopic electric field necessary to obtain a current density of 10 and 1 $mAcm^{-2}$, respectively. If other values are used, it is pointed out.

better performance than that of reported field emitters (see Table 2).

CONCLUSIONS

In conclusion, flexible 3D SnO_2 nanowire arrays have been synthesized on a carbon cloth template. The photoresponse and field emission properties of the hierarchical nanostructure were studied in detail. The photodetector offers a high selectivity toward UV illumination, a fast response speed of less than 0.3 s, and a low dark current of 2.3 pA. Field emission measurements show that a current density of 10 μAcm^{-2} can be obtained by applying a field of 3.3 $V\mu m^{-1}$, and it rises to 1 $mAcm^{-2}$ at a bias field of 4.5 $V\mu m^{-1}$ with a field enhancement factor as high as 2375. It is reasonable to believe that the 3D SnO_2 nanostructure grown by our approach can be used in photodetectors and field emitters. This synthesis strategy is also highly expected to apply to the growth of other semiconductor materials, such as TiO_2 and ZnO, for improved optoelectronic properties.

AUTHOR INFORMATION

Corresponding Author

*E-mail: dkm@suda.edu.cn (K. M. Deng); lli@suda.edu.cn (L. Li).

Notes

The authors declare no competing financial interest.

ACKNOWLEDGMENTS

We thank a Project Funded by the Priority Academic Program Development of Jiangsu Higher Education Institutions (PAPD).

REFERENCES

(1) Xia, Y. N.; Yang, P. D.; Sun, Y. G.; Wu, Y. Y.; Mayers, B.; Gates, B.; Yin, Y. D.; Kim, F.; Yan, H. Q. *Adv. Mater.* **2003**, *15*, 353−389.
(2) Lieber, C. M.; Wang, Z. L. *MRS Bull.* **2007**, *32*, 99−104.
(3) Kind, H.; Yan, H. Q.; Messer, B.; Law, M.; Yang, P. D. *Adv. Mater.* **2002**, *14*, 158−160.
(4) Hu, L. F.; Yan, J.; Liao, M. Y.; Xiang, H. J.; Gong, X. G.; Zhang, L. D.; Fang, X. S. *Adv. Mater.* **2012**, *24*, 2305−2309.
(5) Tsai, D. S.; Lin, C. A.; Lien, W. C.; Chang, H. C.; Wang, Y. L.; He, J. H. *ACS Nano* **2011**, *5*, 7748−7753.
(6) Lin, J.; Huang, Y.; Bando, Y.; Tang, C. C.; Li, C.; Golberg, D. *ACS Nano* **2010**, *3*, 2452−2458.
(7) Wei, X. L.; Bando, Y.; Golberg, D. *ACS Nano* **2012**, *6*, 705−711.
(8) Zhai, T. Y.; Fang, X, S.; Bando, Y.; Liao, Q.; Xu, X. J.; Zeng, H. B.; Ma, Y.; Yao, J. N.; Golberg, D. *ACS Nano* **2009**, *3*, 949−959.
(9) Choi, Y. J.; Hwang, I. S.; Park, J. G.; Choi, K. J.; Park, J. H.; Lee, J. H. *Nanotechnology* **2008**, *19*, 095508.
(10) Kolmakov, A.; Zhang, Y. X.; Cheng, G. S.; Moskovits, M. *Adv. Mater.* **2003**, *15*, 997−1000.
(11) Xu, J. Y.; Ma, L.; Guo, P. F.; Zhuang, X. J.; Zhu, X. L.; Hu, W.; Duan, X. F.; Pan, A. L. *J. Am. Chem. Soc.* **2012**, *134*, 12394−12397.
(12) Li, L.; Wang, H. Q.; Fang, X. S.; Zhai, T. Y.; Bando, Y.; Golberg, D. *Energy Environ. Sci.* **2011**, *4*, 2586−2590.
(13) Tsai, S. H.; Chang, H. C.; Wang, H. H.; Chen, S. Y.; Lin, C. A.; Chen, S. A.; Chueh, Y. L.; He, J. H. *ACS Nano* **2011**, *5*, 9501−9510.
(14) Hsu, C. Y.; Lien, D. H.; Lu, S. Y.; Chen, C. Y.; Kang, C. F.; Chueh, Y. L.; Hsu, W. K.; He, J. H. *ACS Nano* **2012**, *6*, 6687−6692.
(15) Yang, L.; Cheng, S.; Ding, Y.; Zhu, X. B.; Wang, Z. L.; Liu, M. L. *Nano Lett.* **2012**, *12*, 321−325.
(16) Guo, W. X.; Xu, C.; Wang, X.; Wang, S. H.; Pan, C. F.; Lin, C. J.; Wang, Z. L. *J. Am. Chem. Soc.* **2012**, *134*, 4437−4441.
(17) Wang, Z. R.; Wang, H.; Liu, B.; Qiu, W. Z.; Zhang, J.; Ran, S. H.; Huang, H. T.; Xu, J.; Han, H. W.; Chen, D.; Shen, G. Z. *ACS Nano* **2011**, *5*, 8412−8419.
(18) Yuan, C. Z.; Yang, L.; Hou, L. R.; Li, J. Y.; Sun, Y. X.; Hang, X. G.; Shen, L. F.; Lu, X. J.; Xiong, S. L.; Lou, X. W. *Adv. Funct. Mater.* **2012**, *22*, 2560−2566.
(19) Bae, J.; Song, M. K.; Park, Y. J.; Kim, J. M.; Liu, M. L.; Wang, Z. L. *Angew. Chem., Int. Ed.* **2011**, *50*, 1683−1687.
(20) Lu, M. L.; Weng, T. M.; Chen, J. Y.; Chen, Y. F. *NPG Asia Mater.* **2012**, *4*, e26.
(21) Liu, Z. Q.; Zhang, D. H.; Han, S.; Li, C.; Tang, T.; Jin, W.; Liu, X. L.; Lei, B.; Zhou, C. W. *Adv. Mater.* **2003**, *15*, 1754−1757.
(22) Lin, C. H.; Chen, R. S.; Chen, T. T.; Chen, H. Y.; Chen, Y. F.; Chen, K. H.; Chen, L. C. *Appl. Phys. Lett.* **2008**, *93*, 112115−112117.
(23) Hu, L. F.; Yan, J.; Liao, M. Y.; Wu, L. M.; Fang, X. S. *Small* **2011**, *7*, 1012−1017.
(24) Wan, Q.; Dattoli, E.; Lu, W. *Small* **2008**, *4*, 451−454.
(25) Wu, J. M.; Kuo, C. H. *Thin Solid Films* **2009**, *517*, 3870−3873.
(26) Chen, Y. J.; Zhu, C. L.; Cao, M. S.; Wang, T. H. *Nanotechnology* **2007**, *18*, 285502.
(27) Chen, H.; Hu, L. F.; Fang, X. S.; Wu, L. M. *Adv. Funct. Mater.* **2012**, *22*, 1229−1235.
(28) Fang, X. S.; Yan, J.; Hu, L. F.; Liu, H.; Lee, P. S. *Adv. Funct. Mater.* **2012**, *22*, 1613−1622.
(29) Wu, J.; Yu, K.; Li, L. J.; Xu, J. W.; Shang, D. J.; Xu, Y.; Zhu, Z. Q. *J. Phys. D: Appl. Phys.* **2008**, *41*, 185302.
(30) Chen, Y. J.; Li, Q. H.; Liang, Y. X.; Wang, T. H.; Zhao, Q.; Yu, D. P. *Appl. Phys. Lett.* **2004**, *85*, 5682−5684.
(31) He, J. H.; Wu, T. H.; Hsin, C. L.; Li, K. M.; Chen, L. J.; Chueh, Y. L.; Chou, L. J.; Wang, Z. L. *Small* **2006**, *2*, 116−120.
(32) Wang, B.; Yang, Y. H.; Wang, C. X.; Xu, N. S.; Yang, G. W. *J. Appl. Phys.* **2005**, *98*, 073520−073524.
(33) Li, X. B.; Wang, X. W.; Shen, Q.; Zheng, J.; Liu, W. H.; Zhao, H.; Yang, F.; Yang, H. Q. *ACS Appl. Mater. Interfaces* **2013**, *5*, 3033−3041.
(34) Dattoli, E. N.; Wan, Q.; Guo, W.; Chen, Y.; Pan, X.; Lu, W. *Nano Lett.* **2007**, *7*, 2453−2469.
(35) Choi, Y. J.; Hwang, I. S.; Park, J. G.; Choi, K. J.; Park, J. H.; Lee, J. H. *Nanotechnology* **2008**, *19*, 095508.
(36) Lee, S. H.; Jo, G.; Park, W.; Lee, S.; Kim, Y. S.; Cho, B. K.; Lee, T.; Kim, W. B. *ACS Nano* **2010**, *4*, 1829−1836.
(37) Zhang, D. F.; Sun, L. D.; Yin, J. L.; Yan, C. H. *Adv. Mater.* **2003**, *15*, 1022−1025.

(38) Jie, J. S.; Zhang, W. J.; Jiang, Y.; Meng, X. M.; Li, Y. Q.; Lee, S. T. *Nano Lett.* **2006**, *6*, 1887−1892.
(39) Soci, C.; Zhang, A.; Bao, X. Y.; Kim, H.; Lo, Y.; Wang, D. L. *J. Nanosci. Nanotechnol.* **2010**, *10*, 1430−1449.
(40) Li, L.; Zhang, Y.; Fang, X. S.; Zhai, T. Y.; Liao, M. Y.; Sun, X. L.; Koide, Y.; Bando, Y.; Golberg, D. *J. Mater. Chem.* **2011**, *21*, 6525−6530.
(41) Fowler, R. H.; Nordheim, L. *Proc. R. Soc. London A* **1928**, *119*, 173−181.
(42) Xiao, Z. M.; She, J. C.; Deng, S. Z.; Tang, Z. K.; Li, Z. B.; Lu, J. M.; Xu, N. S. *ACS Nano* **2010**, *4*, 6332−6336.
(43) Yuge, R.; Miyawaki, J.; Ichihashi, T.; Kuroshima, S.; Yoshitake, T.; Ohkawa, T.; Aoki, Y.; Iijima, S.; Yudasaka, M. *ACS Nano* **2010**, *4*, 7337−7343.